Time-variant 1D photonic crystals using flowing microdroplets

Zefeng Chen,[1,2,3] Zehui Yong,[1,3] Chi Wah Leung,[1] Xuming Zhang,[1] Yihang Chen,[1,2] Helen L. W. Chan,[1] and Yu Wang[1,*]

[1]*Department of Applied Physics and Materials Research Center, The Hong Kong Polytechnic University, Hong Kong SAR, China*

[2]*Laboratory of Quantum Information Technology, School of Physics and Telecommunication Engineering, South China Normal University, Guangzhou 510006, China*

[3]These authors contributed equally.

**yu.wang@polyu.edu.hk*

Abstract: In this paper we propose a time-variant photonic crystal, which can be formed by a stream of wave-length-scale microdroplets flowing through a microfluidic channel. The functionality stems from the photonic bandgap generated from the 1D periodic perturbation of refractive index. The periodicity, volume fraction and composition of both the dispersed and the continuous phases can be conveniently tuned in real time by hydrodynamic or pneumatic methods. By simulation, it is found that the time-variant nature of the proposed structure can induce an abnormal energy evolution, which is distinct from any existing photonic crystal structures. As a basic component for optofluidic systems, the droplet-based photonic crystal may find potential applications in light modulation and light confinement, and could be an ideal model for pursuing physical insights into time-variant optofluidic systems.

OCIS codes: (230.5298) Photonic crystals; (230.4110) Modulators.

References and links

1. D. Psaltis, S. R. Quake, and C. Yang, "Developing optofluidic technology through the fusion of microfluidics and optics," Nature **442**(7101), 381–386 (2006).
2. C. Monat, P. Domachuk, and B. J. Eggleton, "Integrated optofluidics: a new river of light," Nat. Photonics **1**(2), 106–114 (2007).
3. H. Schmidt and A. R. Hawkins, "The photonic integration of non-solid media using optofluidics," Nat. Photonics **5**(10), 598–604 (2011).
4. P. Y. Chiou, A. T. Ohta, and M. C. Wu, "Massively parallel manipulation of single cells and microparticles using optical images," Nature **436**(7049), 370–372 (2005).
5. S. L. Neale, M. P. MacDonald, K. Dholakia, and T. F. Krauss, "All-optical control of microfluidic components using form birefringence," Nat. Mater. **4**(7), 530–533 (2005).
6. H. Zhu, I. M. White, J. D. Suter, P. S. Dale, and X. Fan, "Analysis of biomolecule detection with optofluidic ring resonator sensors," Opt. Express **15**(15), 9139–9146 (2007).
7. B. S. Schmidt, A. H. Yang, D. Erickson, and M. Lipson, "Optofluidic trapping and transport on solid core waveguides within a microfluidic device," Opt. Express **15**(22), 14322–14334 (2007).
8. A. H. J. Yang, S. D. Moore, B. S. Schmidt, M. Klug, M. Lipson, and D. Erickson, "Optical manipulation of nanoparticles and biomolecules in sub-wavelength slot waveguides," Nature **457**(7225), 71–75 (2009).
9. D. B. Wolfe, R. S. Conroy, P. Garstecki, B. T. Mayers, M. A. Fischbach, K. E. Paul, M. Prentiss, and G. M. Whitesides, "Dynamic control of liquid-core/liquid-cladding optical waveguides," Proc. Natl. Acad. Sci. U.S.A. **101**(34), 12434–12438 (2004).
10. A. Groisman, S. Zamek, K. Campbell, L. Pang, U. Levy, and Y. Fainman, "Optofluidic 1x4 switch," Opt. Express **16**(18), 13499–13508 (2008).
11. Q. Xu, V. R. Almeida, R. R. Panepucci, and M. Lipson, "Experimental demonstration of guiding and confining light in nanometer-size low-refractive-index material," Opt. Lett. **29**(14), 1626–1628 (2004).
12. S. Xiong, A. Q. Liu, L. K. Chin, and Y. Yang, "An optofluidic prism tuned by two laminar flows," Lab Chip **11**(11), 1864–1869 (2011).
13. Z. Li, Z. Zhang, A. Scherer, and D. Psaltis, "Mechanically tunable optofluidic distributed feedback dye laser," Opt. Express **14**(22), 10494–10499 (2006).
14. S. I. Shopova, H. Zhou, X. Fan, and P. Zhang, "Optofluidic ring resonator based dye laser," Appl. Phys. Lett. **90**(22), 221101 (2007).

#172315 - $15.00 USD Received 16 Jul 2012; revised 17 Sep 2012; accepted 3 Oct 2012; published 9 Oct 2012

15. M. Mancuso, J. M. Goddard, and D. Erickson, "Nanoporous polymer ring resonators for biosensing," Opt. Express **20**(1), 245–255 (2012).
16. X. Mao, S.-C. S. Lin, M. I. Lapsley, J. Shi, B. K. Juluri, and T. J. Huang, "Tunable liquid gradient refractive index (L-GRIN) lens with two degrees of freedom," Lab Chip **9**(14), 2050–2058 (2009).
17. Y. Yang, A. Q. Liu, L. K. Chin, X. M. Zhang, D. P. Tsai, C. L. Lin, C. Lu, G. P. Wang, and N. I. Zheludev, "Optofluidic waveguide as a transformation optics device for lightwave bending and manipulation," Nat Commun **3**, 651 (2012).
18. S. Y. Teh, R. Lin, L. H. Hung, and A. P. Lee, "Droplet microfluidics," Lab Chip **8**(2), 198–220 (2008).
19. R. Seemann, M. Brinkmann, T. Pfohl, and S. Herminghaus, "Droplet based microfluidics," Rep. Prog. Phys. **75**(1), 016601 (2012).
20. A. B. Theberge, F. Courtois, Y. Schaerli, M. Fischlechner, C. Abell, F. Hollfelder, and W. T. S. Huck, "Microdroplets in microfluidics: an evolving platform for discoveries in chemistry and biology," Angew. Chem. Int. Ed. Engl. **49**(34), 5846–5868 (2010).
21. M. Prakash and N. Gershenfeld, "Microfluidic bubble logic," Science **315**(5813), 832–835 (2007).
22. T. Thorsen, R. W. Roberts, F. H. Arnold, and S. R. Quake, "Dynamic pattern formation in a vesicle-generating microfluidic device," Phys. Rev. Lett. **86**(18), 4163–4166 (2001).
23. S. L. Anna, N. Bontoux, and H. A. Stone, "Formation of dispersions using flow focusing in microchannels," Appl. Phys. Lett. **82**(3), 364–366 (2003).
24. Y.-C. Tan, J. S. Fisher, A. I. Lee, V. Cristini, and A. P. Lee, "Design of microfluidic channel geometries for the control of droplet volume, chemical concentration, and sorting," Lab Chip **4**(4), 292–298 (2004).
25. E. Um and J.-K. Park, "A microfluidic abacus channel for controlling the addition of droplets," Lab Chip **9**(2), 207–212 (2009).
26. G. F. Christopher, J. Bergstein, N. B. End, M. Poon, C. Nguyen, and S. L. Anna, "Coalescence and splitting of confined droplets at microfluidic junctions," Lab Chip **9**(8), 1102–1109 (2009).
27. L. Dong, A. K. Agarwal, D. J. Beebe, and H. Jiang, "Adaptive liquid microlenses activated by stimuli-responsive hydrogels," Nature **442**(7102), 551–554 (2006).
28. M. Hashimoto, B. Mayers, P. Garstecki, and G. M. Whitesides, "Flowing lattices of bubbles as tunable self-assembled diffraction gratings," Small **2**(11), 1292–1298 (2006).
29. L. K. Chin, A. Q. Liu, J. B. Zhang, C. S. Lim, and Y. C. Soh, "An on-chip liquid tunable grating using multiphase droplet microfluidics," Appl. Phys. Lett. **93**(16), 164107 (2008).
30. L. K. Chin, A. Q. Liu, Y. C. Soh, C. S. Lim, and C. L. Lin, "A reconfigurable optofluidic Michelson interferometer using tunable droplet grating," Lab Chip **10**(8), 1072–1078 (2010).
31. S. K. Y. Tang, Z. Li, A. R. Abate, J. J. Agresti, D. A. Weitz, D. Psaltis, and G. M. Whitesides, "A multi-color fast-switching microfluidic droplet dye laser," Lab Chip **9**(19), 2767–2771 (2009).
32. E. Castro-Hernández, W. van Hoeve, D. Lohse, and J. M. Gordillo, "Microbubble generation in a co-flow device operated in a new regime," Lab Chip **11**(12), 2023–2029 (2011).
33. L. Shui, E. S. Kooij, D. Wijnperle, A. van der Berg, and J. C. T. Eijkel, "Liquid crystallography: 3D microdroplet arrangements using microfluidics," Soft Matter **5**(14), 2708–2712 (2009).
34. L. Shui, A. van den Berg, and J. C. T. Eijkel, "Scalable attoliter monodisperse droplet formation using multiphase nano-microfluidics," Microfluid. Nanofluid. **11**(1), 87–92 (2011).
35. S. Xiong, Y. Yang, K. Mawatari, T. Kitamori, and A. Q. Liu, "Nano-optofluidic droplet via photonic crystal characters for bio-imaging and detection applications," in *The 15th International Conference on Miniaturized Systems for Chemistry and Life Sciences*, pp. 1077–1079 (2011).
36. P. S. Dittrich and A. Manz, "Lab-on-a-chip: microfluidics in drug discovery," Nat. Rev. Drug Discov. **5**(3), 210–218 (2006).
37. E. Brouzes, M. Medkova, N. Savenelli, D. Marran, M. Twardowski, J. B. Hutchison, J. M. Rothberg, D. R. Link, N. Perrimon, and M. L. Samuels, "Droplet microfluidic technology for single-cell high-throughput screening," Proc. Natl. Acad. Sci. U.S.A. **106**(34), 14195–14200 (2009).
38. M. T. Guo, A. Rotem, J. A. Heyman, and D. A. Weitz, "Droplet microfluidics for high-throughput biological assays," Lab Chip **12**(12), 2146–2155 (2012).
39. H. Kogelnik, "An introduction to integrated optics," IEEE Trans. Microw. Theory Tech. **23**(1), 2–16 (1975).
40. J. D. Joannopoulos, R. D. Meade, and J. N. Winn, *Photonic Crystals: Molding the Flow of Light* (Princeton Univ. Press, Princeton, 1995).
41. A. Taflove and S. C. Hagness, *Computational Electrodynamics: The Finite-Difference Time-Domain Method* (Artech: Norwood, MA, 2000).
42. A. F. Oskooi, D. Roundy, M. Ibanescu, P. Bermel, J. D. Joannopoulos, and S. G. Johnson, "Meep: A flexible free-software package for electromagnetic simulations by the FDTD method," Comput. Phys. Commun. **181**(3), 687–702 (2010).
43. Carbon disulifide (CS_2) sometimes can be used as infrared transparent solvent, whose transparent window mainly spans at wavelengths from 8 to16μm. We select it because of its high refractive index which is 1.628. The most popular infrared solvent is carbon tetrachloride (CCl_4), which is transparent at all wavelength less than 12μm. Other infrared transparent solvents include tetrachloroethylene, chloroform, dimethylformamide, dioxane, cyclohexane and benzene.
44. J. S. Forsi, P. R. Villeneuve, J. Ferrera, E. R. Thoen, G. Steinmeyer, S. Fan, J. D. Joannopoulos, L. C. Kimerling, H. I. Smith, and E. P. Ippen, "Photonic bandgap microcavities in optical waveguides," Nature **390**, 143–145 (1999).
45. K. J. Vahala, "Optical microcavities," Nature **424**(6950), 839–846 (2003).

#172315 - $15.00 USD Received 16 Jul 2012; revised 17 Sep 2012; accepted 3 Oct 2012; published 9 Oct 2012

46. Y. A. Vlasov, M. O'Boyle, H. F. Hamann, and S. J. McNab, "Active control of slow light on a chip with photonic crystal waveguides," Nature **438**(7064), 65–69 (2005).
47. V. Lien and F. Vollmer, "Microfluidic flow rate detection based on integrated optical fiber cantilever," Lab Chip **7**(10), 1352–1356 (2007).
48. J. Homola, S. S. Yee, and G. Gauglitz, "Surface plasmon resonance sensors: review," Sens. Actuators B **54**(1-2), 3–15 (1999).
49. S. Jakiela, S. Makulska, P. M. Korczyk, and P. Garstecki, "Speed of flow of individual droplets in microfluidic channels as a function of the capillary number, volume of droplets and contrast of viscosities," Lab Chip **11**(21), 3603–3608 (2011).
50. J. G. Cuennet, A. E. Vasdekis, L. De Sio, and D. Psaltis, "Optofluidic modulator based on peristaltic nematogen microflows," Nat. Photonics **5**(4), 234–238 (2011).
51. J. Lee, H. Park, J. Jung, and H. Kwak, "Bubble nucleation micro line heaters," J. Heat Transfer **125**(4), 687–692 (2003).
52. K. Zhang, A. Jian, X. Zhang, Y. Wang, Z. Li, and H. Y. Tam, "Laser-induced thermal bubbles for microfluidic applications," Lab Chip **11**(7), 1389–1395 (2011).
53. According to ideal gas law, a heat source at a fixed location will enlarge the volume of microbubbles as they flow through.
54. J.-M. Lim, J. P. Urbanski, T. Thorsen, and S.-M. Yang, "Pneumatic control of a liquid-core/liquid-cladding waveguide as the basis for an optofluidic switch," Appl. Phys. Lett. **98**(4), 044101 (2011).
55. W. Song and D. Psaltis, "Pneumatically tunable optofluidic 2×2 switch for reconfigurable optical circuit," Lab Chip **11**(14), 2397–2402 (2011).

1. Introduction

Optofluidics is an emerging field that holds strong promises to revitalize many conventional systems and to enable new functionalities [1–3]. On one hand, it introduces optical means of maneuverings and sensing of microfluids, as well as particles, analytes therein [4–8]; on the other hand, it adds reconfigurability, tunability, and a full gamut of compositional options (mainly about refractive indices) into integrated optics [9–17]. In the case of light manipulation, laminar flows have been used for a long time [9]. For flows confined within micrometer scale, viscous forces dominate over inertial forces (as indicated by a low Reynolds number), thus the multiphase microflows never mix violently (as that in turbulent flow) but only diffuse a little into each other, which can be precisely controlled by the flow rate. A large variety of devices have been implemented based on this principle, such as optical switches [9, 10], liquid waveguides [9, 11], prisms [12], resonators and dye lasers [13–15]. Gradient-index materials can also be realized in microfluidic systems, which cannot be easily produced in solid state systems [16, 17].

The major limitation of continuous flow is the number of functions it can undertake, which is restricted by the channel geometry adopted *a priori*. In droplet microfluidics however, enabled by discrete volumes separated by immiscible phases, multiple functions can be cascaded along the channel geometry (that's why it is also called "digital microfluidics") [18–20]. A typical demonstration of this property is the bubble logic, where bubbles experience selective splitting or combination along complex channel structures, which is analogue to digital signals in AND/OR gates [21]. Moreover, many properties such as size, shape, monodispersity, periodicity can be finely controlled by simple T-junction [22] or flow-focusing methods [23]. Droplets thus generated can also be processed into a series of splitting, combination or mixes to provide more versatility [21, 24–26]. This platform can provide femto- to pico-liter environments for important chemical reactions, synthesis and encapsulation of biomolecules, drug delivery, etc [18–20].

All the benefits mentioned above have heralded a bright prospect in synergy of droplets and optics. Actually, in some designs, droplet lenses with tunable interfacial surfaces have been built [27]. Other researchers have developed droplet-based optical gratings which can be applied in Michelson interferometer and optical sensors [28–30]. Besides, by exploiting the flowing feature of the droplets, a multi-color fast-switching dye laser has been constructed [31]. Despite of these interesting results, there is still plenty of room for development of droplet-based optofluidic systems. For example, droplets formed in microchannels (either by T-junction methods or flow-focusing method) are inherently periodic, a feature that is analogue to 1D photonic crystals (and hence some similar behaviors like photonic bandgaps and defect tunneling). However, technical difficulties in generation of ultra-small wavelength-scale

#172315 - $15.00 USD Received 16 Jul 2012; revised 17 Sep 2012; accepted 3 Oct 2012; published 9 Oct 2012

droplets have impeded the burgeoning of this area. Recently, Castro-Hernandez et al. reported a method for controllable microbubble generation with diameters less than 5μm and polydispersity indices below 5% [32]. Surfactants-assisted oil-phase nanodroplets have also been reported [33–35]. With the aid of the fast development in digital microfluids from medicine requirements, one can predict a continuous miniaturization of droplets, which could make it possible to construct practically useful optofluidic systems [36–38].

In this article, we propose the idea of employing periodically aligned droplets to form photonic crystals with a flowing nature (which we may call it as time-variant photonic crystal (TvPC)). Our simulations demonstrate that such system exhibit interesting optical behaviors which can be tuned by changing the droplet shape, configuration, volume fraction and so on. Optical modulation as well as dynamic light confinements is also discussed.

2. Models and theories

2.1 Droplet-based 1D photonic crystal

Figure 1 shows a schematic illustration for the proposed droplet-based 1D photonic crystal (PC) waveguide. The microchannel is bent in a U-shaped structure, where light can be guided in at one end, and guided out at the other. In a typical microfluidic waveguide, light transmits through the fluids by index-guiding (when fluids have a higher refractive index (RI) than its cladding) [9, 39]. In our case, a stream of microdroplets distributed periodically is injected to flow through the channel, either by flow-focusing or T-junction methods. The periodic perturbations of RI therefore bring in a photonic bandgap, as discussed below.

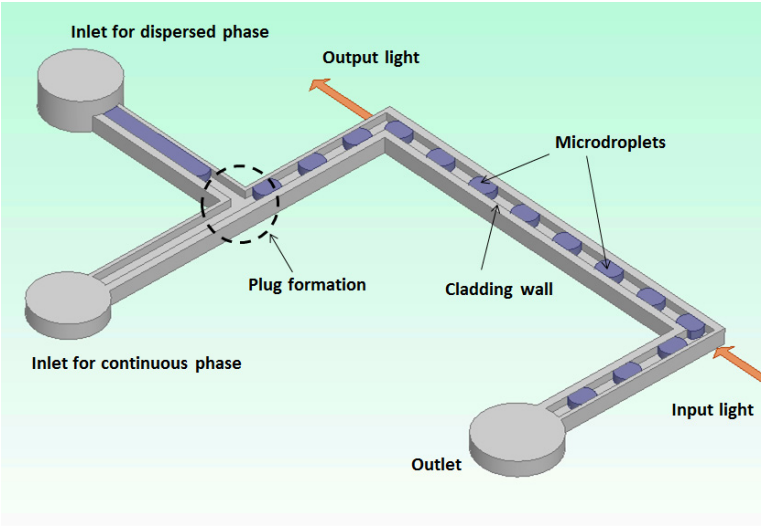

Fig. 1. Schematic illustration of droplet-based U-shape PC waveguide.

The general wave field in the droplet-infused waveguide can be described as [40]:

$$\nabla\times[n(x)]^{-2}\nabla\times e^{ik\cdot r}E_k(x)=(\omega(k)/c)^2 e^{ik\cdot r}E_k(x), \qquad (1)$$

where $n(x) = n(x + R)$ describes the periodic RI change in the waveguide, k is the wave vector along the channel, R is the spatial period of RI, ω is angular frequency, $E_k(x)$ is the electric wave function. Figure 2 illustrated different dispersion curves of the two waveguides, the latter of which correspond to droplet-based 1D PCs. One can see obviously the splitting of guided modes caused by the perturbation introduced by microdroplets, while the gap width is directly related to the RI contrast.

#172315 - $15.00 USD Received 16 Jul 2012; revised 17 Sep 2012; accepted 3 Oct 2012; published 9 Oct 2012

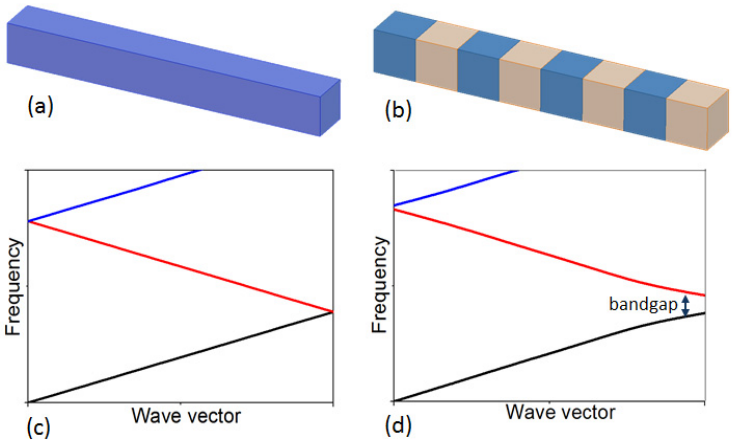

Fig. 2. (a) Normal index-guiding waveguide. (b) Waveguide with periodic modulation of RI. (c) Linear dispersion curve in (a). (d) Splitting of the waveguide modes in (b).

2.2 FDTD analysis on the transmission properties

2D FDTD method [41] has been performed to investigate the transmission property of the TvPC structure, using a freely available software package [42]. The model is constructed as described in Fig. 3(a). The microchannel is defined to be of width a (hereinafter we take a to be the unit length to avoid specified units), while PDMS of thickness $0.2a$ are defined aside the edges of the channel, as cladding walls [43]. Perfect matched layers (PML) are assumed at the boundaries to resemble an electromagnetic open environment. To provide some practical guidance, we take the continuous phase to be carbon disulfide (CS_2) with RI of 1.628 since it is transparent in certain infrared window [43]. Dispersed phase is chosen to be microbubbles (RI = 1) due to its relative high RI contrast against the liquid media. The lengths of the microbubbles are $1.4a$, and the spatial period R between two bubbles is $2.6a$. Curved two-phase interfaces are also considered. The contact angle between bubbles and PDMS wall is set to be 45°.

As demonstrated in Fig. 3(a), when the numerical process is launched, the waveguide is excited outside the left end of the channel by a light source. The transmittance therefore can be detected at the observer point. The source is actually taken to be Gaussian-like, TE-polarized and with a beamwidth equal to the channel width a. The transmittance is calculated as the ratio between transmitted and incident electric flux of the TvPC waveguide, as

$$T = \int |E|^2 dl \,/\, \int |E_0|^2 dl, \tag{2}$$

where dl means to integrate along the end cross section at the observer point, E is the E-field recorded at the observer point of TvPC, and E_0 is the E-field for reference which approximately equals to the incident field. Practically it is taken to be the transmitted E-field for an empty waveguide without microbubbles, as shown in Fig. 3(b).

#172315 - $15.00 USD Received 16 Jul 2012; revised 17 Sep 2012; accepted 3 Oct 2012; published 9 Oct 2012

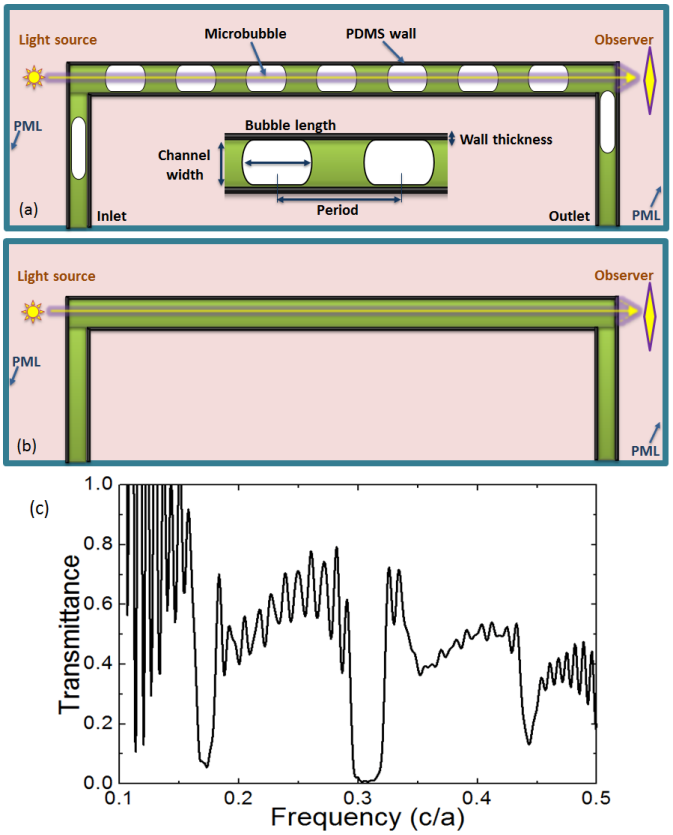

Fig. 3. The two-dimensional FDTD model and results of the TvPC structure. (a) The model of as-proposed droplet-based TvPC waveguide for calculation. (b) The empty waveguide model for reference. (c) The transmittance vs. frequency observed at the output point when the waveguide is excited at the light source point.

Figure 3(c) shows the calculated transmittance derived as stated above. Despite the impairments caused by curved two-phase interfaces and cladding walls, the bandgap remains prominent as those derived from 1D PC theory (one centred at 0.17*c/a*, and the other centred at 0.31*c/a*, where *c* is the speed of light in vacuum). It is obvious that, when microbubbles are present, the transmission is blocked at the frequency of interest, forming a photonic bandgap. Unlike conventional solid-state PCs, the proposed structure is highly reconfigurable that, the bandgap is always ready for change, which can be conveniently controlled by altering compositions or flow rates in the microfluidic channel.

3. Results and discussions

3.1 Energy evolution in droplet-based TvPC

What is most interesting is the flowing nature of the distribution of microdroplets, which introduces time-variant properties that have not been observed in existing solid-state PCs [44–46]. In the proposed TvPC, the RI distribution is actually a function of time *t*, as $n(x,t) = n(x-R,t-T)$, where *R* is the spatial period (i.e., the distance between two adjacent microdroplets), $T = R/v$ is the time period for a TvPC to restore its configuration as the stream of microdroplets flows forward, and *v* is the speed of flow. Therefore, as in the model defined in the former section, the distribution of microbubbles will be different at different times in a period *T*. Since the electromagnetic energy tends to concentrate at high RI region (where microbubbles are absent) [40], the energy distribution rolls periodically as time goes.

#172315 - $15.00 USD Received 16 Jul 2012; revised 17 Sep 2012; accepted 3 Oct 2012; published 9 Oct 2012

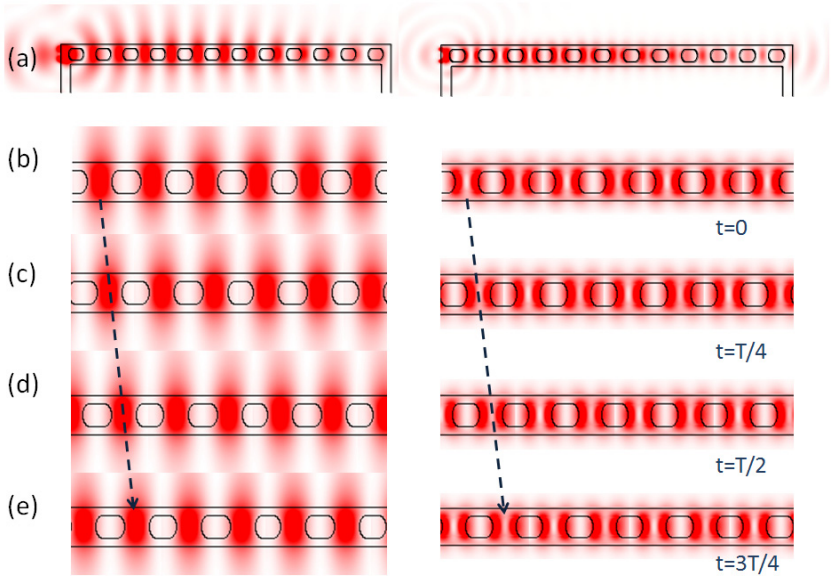

Fig. 4. Energy evolution in droplet-based 1D TvPC. (a) The energy distributions in a finite TvPC at the 1st and the 2nd order waveguide modes, respectively. The waveguide is excited by a continuous source outside the left end of the channel. (b)-(e) The 1st and 2nd order energy distributions in an infinite 1D droplet-based TvPC at (b) $t = 0$, (c) $t = T/4$, (d) $t = T/2$ and (e) $t = 3T/4$, where T is the time period for the TvPC to restore. The dashed arrows indicate the evolution of electromagnetic energy, along with the flow of microbubbles.

To explore the properties discussed above, we have calculated the energy distributions under different conditions. First we consider the situation in a finite TvPC waveguide, with 12 microbubbles aligned periodically in the microchannel, as shown in Fig. 4(a). The two graphs are generated at different frequency points, which correspond to the 1st and the 2nd order waveguide mode, respectively. At the 1st order waveguide mode, the wavelength of the light is generally the double of the bubble period R. In this case, electromagnetic energies do concentrate at high RI index as predicted, except at regions near the end of the channel. At the 2nd order waveguide mode however, the concentration of energy is blurred, mainly at the edges of microbubbles, since there are two amplitude peaks between adjacent bubbles for light of wavelength equals to R. Figure 4(b)-(e) show energy distribution in an infinite TvPC waveguide at different times in a time period T. As bubbles flow through the channel, it is obvious that the energy concentration evolves (as indicated by the dashed arrows), and hence experiences a periodic modulation (the peculiarity of this phenomenon will be demonstrated later).

3.2 General features

We then consider the influence induced by the droplet sizes and the solute analytes. At first the effects of different droplet sizes are considered. Figure 5 shows that the optimal length of microbubbles is $1.2a$, where the bandwidth is the widest and the gap depth is –46dB. As this length grows, the gap frequency shifts to higher because the effective RI gets smaller. However, when the bubble fraction is too large to maintain a significant RI contrast, the bandgap vanishes completely. Practically, the average size of microbubbles can be determined by flow rate and viscosities, as $d\mu(Q_g/Q_l)^{\beta}(\mu_g/\mu_l)^{g}$, where β ranges from 0.3 to 0.5 under different conditions [32], Q_g and Q_l indicate the gas and liquid flow rates, μ_g and μ_l are gas and liquid viscosities, respectively. It means this bandgap feature is quite agile to the rate and viscosity of the microfluidic configurations, which may provide many functions such as flow control calibration [47].

#172315 - $15.00 USD Received 16 Jul 2012; revised 17 Sep 2012; accepted 3 Oct 2012; published 9 Oct 2012

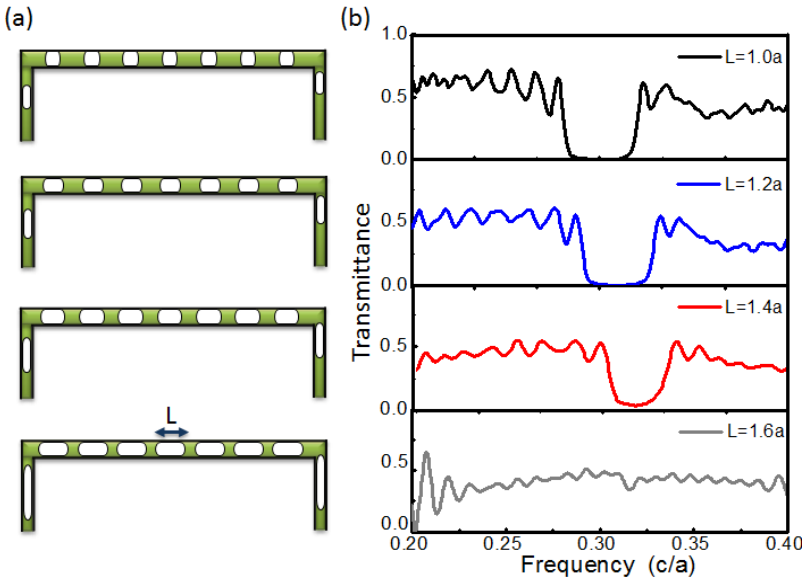

Fig. 5. Relationships between transmittance and lengths of microbubbles. (a) Schematic illustration of different microbubble sizes *L*. (b) The transmittance spectra of the 1D TvPC waveguide for different microbubble lengths, of 1.0*a*, 1.2*a*, 1.4*a*, 1.6*a*, respectively.

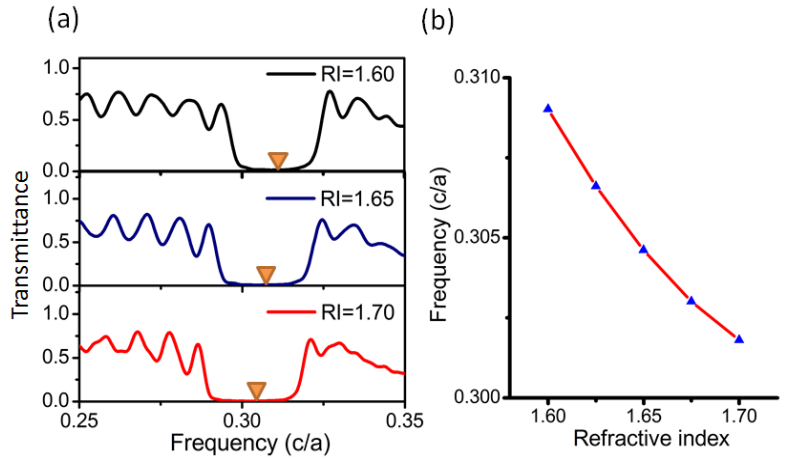

Fig. 6. Relationships between transmittance and RI of continuous phase adopted in droplet-based 1D TvPCs (a) The transmittance of TvPC with different RIs, where center frequencies of the bandgaps are marked by orange triangles. (b) The center frequency of the bandgap as a function of RIs.

Slight RI changes can be caused by solute analytes or other gradients incorporated in the microfluids. Sensitivities to such changes have been adopted in many chemical sensor applications [48]. The same effect is also considered in droplet-based TvPCs. As shown in Fig. 6, the resultant shift of transmission spectra is fairly prominent. It is obvious that the center frequency of the bandgap increases as the RI decreases.

3.3 Light modulation by droplet-based TvPC

The possible modulation of light was also investigated. As explained earlier, the time-variant nature of the droplet-based PC inevitably brings in an energy evolution, which can be directly observed at the output end of the waveguide. In our models, we consider a TvPC where a

#172315 - $15.00 USD Received 16 Jul 2012; revised 17 Sep 2012; accepted 3 Oct 2012; published 9 Oct 2012

stream of 9 bubbles is formed periodically aligned along a U-shape microchannel (geometries are the same as described in section 2.2). If the flow speed is v, then it takes $T = 2.6a/v$ for the TvPC to restore its configuration, and $1.4a/v$ for a microbubble to pass over. It is obvious that, the energy experiences a periodic modulation as the TvPC flows and restores. However, the exact conditions within a period T are rather complicated.

Figure 7(a) demonstrates 4 snapshots of energy distributions at the output end of the TvPC, from which we can try to explain the modulation behavior in a phenomenological way. From the pictures, we can see the operating frequency considered at this time is within the 2nd waveguide mode, since there are two concentration points between adjacent microbubbles. Both of them are located at the interfaces between bubbles and liquids. Intuitively, since the light tends to concentrate at interfaces, the output transmittance will be enhanced when a bubble is closely approaching the corner point or has just left there and turned downwards. As assumed in the pictures, at $t = 0$, the distance for the closest bubble to meet the corner point is about $1.3a$. At this distance there are no concentration points covering the channel edge, thus the intensity at the edge is dilute. After a short period of $T/4$, the border of the bubble meets the corner point, while taking along the concentration point at the interface; hence the transmittance increases. At $t = T/2$, the bubble is leaving the corner point; just one half of it is within the light path; hence the transmittance decreases again. The last condition at $t = 3T/4$ is very similar to that at $T/4$. Finally, after a time of T, the TvPC restores its original state, and then starts a new cycle.

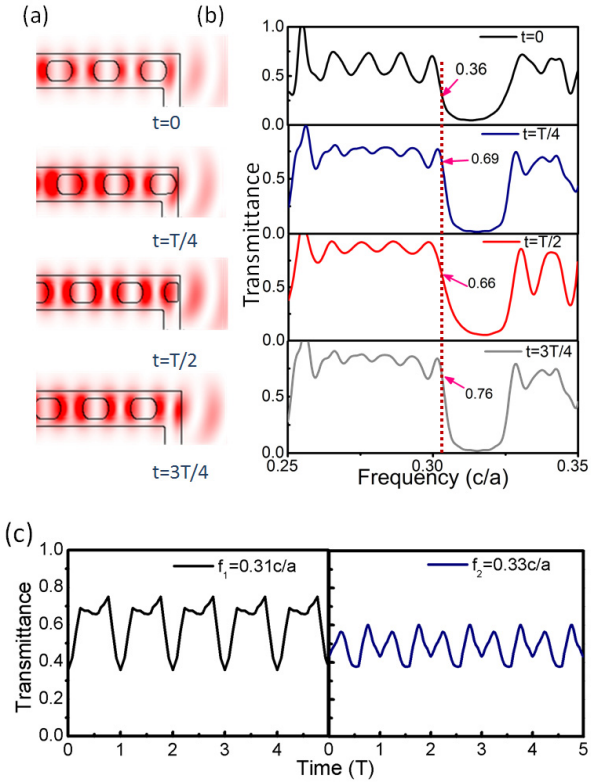

Fig. 7. Light modulation at the bandedge frequency of the droplet-based 1D TvPC. (a) The energy evolution at the frequency $f = 0.31c/a$, in a time period T. (b) The transmission spectra of the waveguide at $t = 0$, $t = T/4$, $t = T/2$, $t = 3T/4$, respectively. (c) The transmittance modulation at $f_1 = c/a$, $f_2 = 0.33c/a$, respectively, as a function of time from 0 to $5T$.

#172315 - $15.00 USD Received 16 Jul 2012; revised 17 Sep 2012; accepted 3 Oct 2012; published 9 Oct 2012

The calculated transmittance spectra at $t = 0$, $t = T/4$, $t = T/2$ and $t = 3T/4$ are plotted in Fig. 7(b). The dashed red line marks the frequency $f_1 = 0.31c/a$, which is just the frequency adopted in energy plotting in Fig. 7(a). It is obviously seen in this picture that, at different frequencies, the output transmittances change their values following different routes. Particularly, the transmittances at bandedge points oscillate most heavily. However, since the basic periodicity and bubble sizes do not change, the bandgap features, i.e., the center frequency and bandwidth remain unchanged as time evolves.

To illustrate the overall light modulation, we have studied 13 models with different bubble distributions within a time period T. The transmittances as a function of time are plotted in Fig. 7(c) at two frequencies, $f_1 = c/a$, and $f_2 = 0.33c/a$. "M-shaped" waveforms are clearly seen in both graphs, where the maximum values at the shoulders of the "M" correspond exactly to the two concentration points between adjacent microbubbles.

A prominent advantage in this method of light modulation is that, the period of modulation $T = R/v$, is directly related to the geometry of bubbles and flow rate, which can be easily tuned hydraulically [24, 49, 50], and controlled in real-time.

3.4 Static and dynamic light confinements in TvPC

The as-proposed droplet-based TvPC waveguide is also investigated when defects are introduced. Just as in 1D solid-state PCs, if there is a defect in a photonic crystal, the electromagnetic wave at certain frequencies will be confined in the defect and excite a defect mode which can tunnel energy through the photonic crystal [43, 44]. In droplet-based TvPCs, a defect can be generated by either a larger bubble or a longer liquid section. Static defects can be stabilized by a nano-sized resistive heater [51], or a laser induced method [52, 53], while dynamic defects can be generated and controlled hydraulically [24, 49], or pneumatically [54, 55].

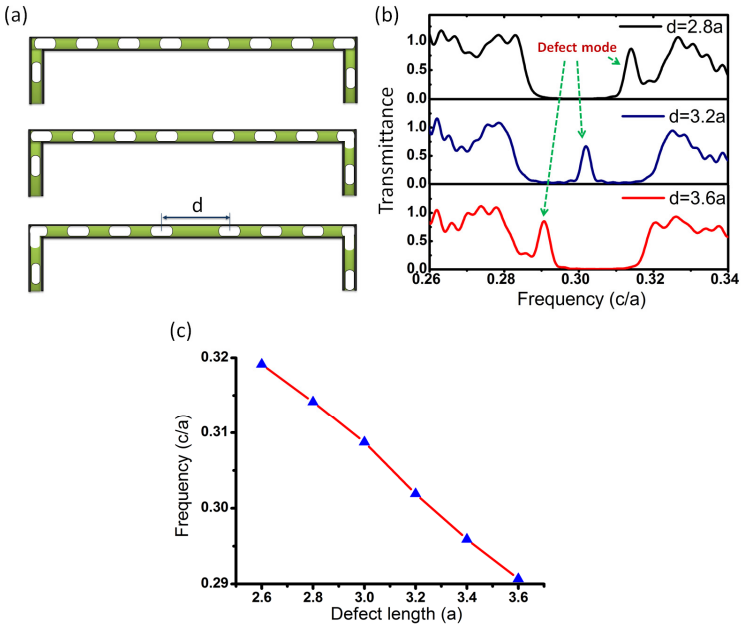

Fig. 8. Relationships between defect lengths and defect mode frequencies. (a) Schematic models showing different defective TvPCs produced by inserting a longer liquid section at the center. The defect length d is defined to be the distance between two bubbles closest to the center. (b) The transmittance spectra of the defective TvPC, where the dashed arrows indicate the shifts of the defect mode by variation of d. (c) The plot of defect mode frequency as a function of defect length.

#172315 - $15.00 USD Received 16 Jul 2012; revised 17 Sep 2012; accepted 3 Oct 2012; published 9 Oct 2012

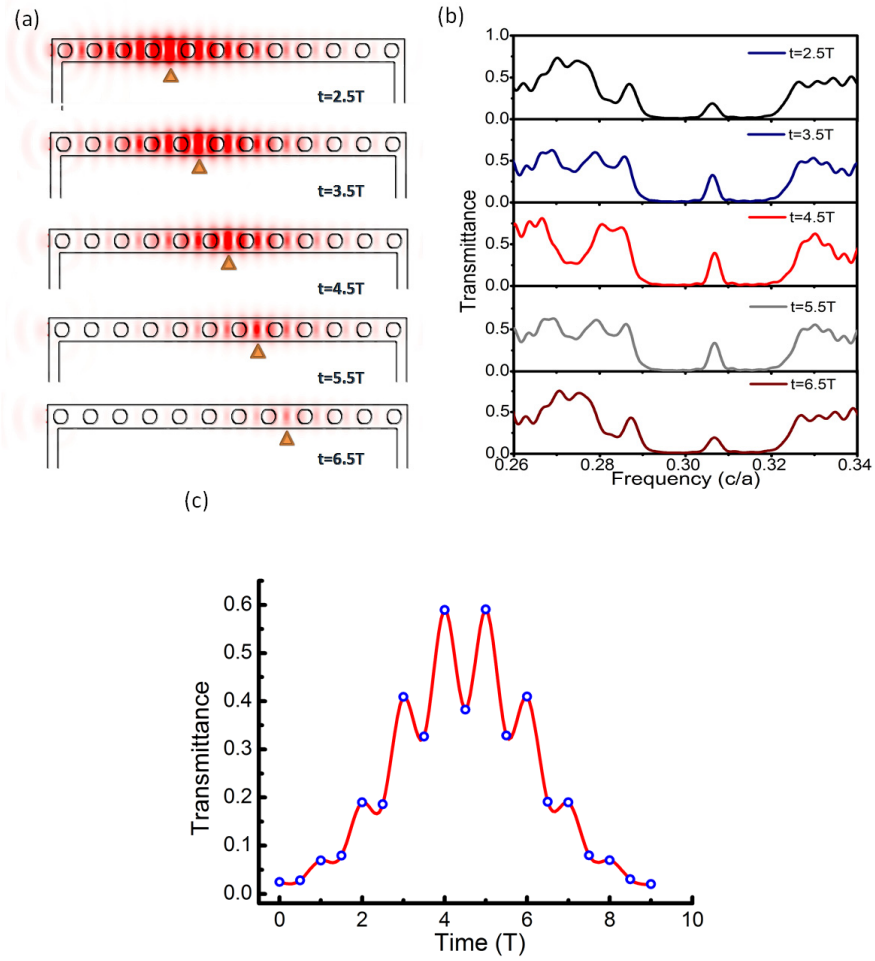

Fig. 9. Behaviors of dynamic defects in droplet-based 1D TvPC. (a) Electromagnetic energy distribution in a defective TvPC waveguide at $t = 2.5T$, $t = 3.5T$, $t = 4.5T$, t = 5.5T and $t = 6.5T$, the defect length is 3.2a. The points with highest energy density are marked by orange triangles. (b) Transmittance spectra of the defective TvPC, where the defect mode peaks are clearly shown. (c) The transmittance at the defect mode frequency as a function of time, from 0 to 9T, the period for a dynamic defect to flow through the TvPC structure; blue circles are data points, and the red line is only guide for eyes.

Figure 8 shows the relationship between defect lengths and defect mode frequencies. As shown in Fig. 8(a), the model we study now are almost the same with the models described earlier, except the bubble length is changed to 1.2a. Besides, a longer liquid section is present at the center of the TvPC waveguide, with a defect length d defined to be the distance between the two bubbles closest to the center. The three pictures demonstrate three different structures with d = 2.8a-3.6a. Figure 8(b) shows the transmission spectra of the defective TvPC waveguide with different defect lengths as indicated in Fig. 8(a), where the shifts of the defect mode are indicated by dashed arrows. Figure 8(c) shows that the defect mode frequency obeys a negative linear relationship with the defect length. This property actually can be applied in optical components like frequency-tunable filter.

Now we discuss a unique property that has never been observed in any existing solid-state PCs, the dynamic defects. This time, the defect length d is set fixed as 3.2a. However, the position of the defect is not fixed. In this scenario, the longer liquid section is generated elsewhere before the stream of microbubbles enters into the U-shaped TvPC waveguide. Figure 9(a) is the energy distribution in the waveguide at different times, where $t = 0$ corresponds to

#172315 - $15.00 USD Received 16 Jul 2012; revised 17 Sep 2012; accepted 3 Oct 2012; published 9 Oct 2012

the time when the defect is located between the first two bubbles at the left end, and T is still the time period for a non-defective TvPC to restore. Not surprisingly, there is an obvious light confinement in the defect area. Accordingly, the transmission spectrum at the output end reveals a defect mode (Fig. 9(b)). Along with the movement of the stream of microbubbles, the confined light also moves towards the right end, as time goes by. However, the frequency of defect mode does not change, because of the fixed defect length.

Besides, from Fig. 9(a) one can also see that, the amplitude of the light confinement diminishes quickly as the defect approaches the right end. Since the light source is located at the left side, the defect mode is harder to be excited when it is too far. However, the transmittance does not diminish in accordance. In Fig. 9(b), we can observe that the transmittance at the defect mode achieve its "maximum" at $t = 4.5T$, when the defect is at the center of the TvPC. This can be explained by coupled cavity theory — the tunneling effect achieve its maximum value when the two attenuation coefficients τ_1 and τ_2 are equal to each other, where τ_1 and τ_2 correspond to different attenuation rates to the left and right exterior region, respectively [40].

The transmittance at the defect mode frequency as a function of time (from 0 to $9T$) is shown in Fig. 9(c). The diagram actually revealed a saw-teeth-shaped pulse signal, corresponding to the passing through of the defect made by the longer liquid section. Additionally, the curve is heavily modulated by "M-shaped" fluctuations, which are caused by single bubbles as discussed previously. Such effect is prominent in Fig. 9(c), it shifts the maximum transmittance to $t = 4T$ and $5T$ instead of the ideal position $t = 4.5T$.

5. Conclusion

In this work, we have proposed the concept of time-variant photonic crystals, which not only offers total reconfigurability, but also introduces new features, like time-variant refractive index, and evolution of energy distribution. As one of the possible realizations, a U-shaped droplet-based 1D TvPC waveguide has been proposed. We have also investigated the effects of droplet sizes and compositions in this structure. Besides, some practical designs, like light modulation by the evolution of energy distribution, and light confinement by static or dynamic defects have also been discussed.

Since the features of the TvPCs, particularly the nature of flowing, are not present in any solid-state photonics, the TvPCs make open up new applications of optofluidics. We hope this work will inspire further research on theoretical and experimental studies of dynamic optofluidics.

Acknowledgment

This work was supported by the Hong Kong Polytechnic University (Projects 1-ZV5K & J-BB9P).

#172315 - $15.00 USD Received 16 Jul 2012; revised 17 Sep 2012; accepted 3 Oct 2012; published 9 Oct 2012